Model-Based Compliance Discrimination via Soft Tactile Optical Sensing and Optical Flow Computation: A Biomimetic Approach

Giulia Pagnanelli, *Graduate Student Member, IEEE*, Simone Ciotti, Nathan Lepora, *Member, IEEE*, Antonio Bicchi, *Fellow, IEEE*, and Matteo Bianchi, *Member, IEEE*

***Abstract*—Soft tactile optical sensors have opened up new possibilities for endowing artificial robotic hands with advanced touch-related properties; however, their use for compliance discrimination has been poorly investigated and mainly relies on data-driven methods. Discrimination of object compliance is crucial for enabling accurate and purposeful object manipulation. Humans retrieve this information primarily using the contact area spread rate (CASR) over their fingertips. CASR can be defined as the integral of tactile flow, which describes the movement of iso-strain surfaces within the fingerpad. This work presents the first attempt to discriminate compliance through soft optical tactile sensing based on a computational model of human tactile perception that relies on CASR and tactile flow concepts. To this aim, we used a soft optical biomimetic sensor that transduces surface deformation via movements of marked pins, similar to the function of intermediate ridges in the human fingertip. We acquired images of markers' movements during the interaction with silicone specimens with different compliance at different indenting forces. Then, we computed the optical flow as a tactile flow approximation and its divergence to estimate the CASR. Our model-based approach can accurately discriminate the compliance levels of the specimens, both when the sensor probed the surface perpendicularly and with different inclinations. Finally, we used the relation between specimen compliance and the experimentally evaluated CASR to infer the compliance of a new specimen relying on the estimated CASR.**

***Index Terms*—Force and tactile sensing, perception for grasping and manipulation, soft sensors and actuators.**

Manuscript received 1 April 2023; accepted 15 August 2023. Date of publication 28 August 2023; date of current version 6 September 2023. This letter was recommended for publication by Associate Editor C. Cao and Editor Y.-L. Park upon evaluation of the reviewers' comments. This work was supported in part by the EU Horizon 2020 Research and Innovation Program under Grant 871237 (Sophia), in part by the European Research Council (ERC) under Grant 810346 (Natural BionicS), in part by the Italian Ministry of Education and Research (MIUR) in the framework of the ForeLab Project and of the CrossLab Project (Departments of Excellence), in part by PRIN (Programmi di Ricerca Scientifica di Rilevante Interesse Nazionale) 2017 through Project TIGHT: Tactile InteGration for Humans and arTificial systems under Grant 2017SB48FP, and in part by the European Union by the Next Generation EU Project ECS00000017 'Ecosistema dell'Innovazione' Tuscany Health Ecosystem (THE, PNRR, Spoke 9: Robotics and Automation for Health). *(Corresponding author: Giulia Pagnanelli.)*

Giulia Pagnanelli and Matteo Bianchi are with Centro di Ricerca "Enrico Piaggio", Universita' di Pisa, 56126 Pisa, Italy, and also with the Dipartimento di Ingegneria dell'Informazione, Universita' di Pisa, 56126 Pisa, Italy (e-mail: giulia.pagnanelli17@gmail.com; matteobianchi23@gmail.com).

Simone Ciotti is with the Dipartimento di Ingegneria dell'Informazione, Universita' di Pisa, 56126 Pisa, Italy (e-mail: ciottisimone88@gmail.com).

Nathan Lepora is with the Department of Engineering Mathematics - Bristol Robotics Laboratory, University of Bristol, BS8 1TW Bristol, U.K. (e-mail: n.lepora@bristol.ac.uk).

Antonio Bicchi is with the Centro di Ricerca "Enrico Piaggio", Universita' di Pisa, 56126 Pisa, Italy, and with the Dipartimento di Ingegneria dell'Informazione, Universita' di Pisa, 56126 Pisa, Italy, and also with the Soft Robotics for Human Cooperation and Rehabilitation, Istituto Italiano di Tecnologia, 16163, Genova, Italy (e-mail: antonio.bicchi@iit.it).

Digital Object Identifier 10.1109/LRA.2023.3309576

I. Introduction

THE sense of touch is essential for humans to explore and interact with the world. It helps us access important object characteristics such as size, shape, weight, and compliance. Compliance and its subjective perceptual counterpart, softness, are important physical properties of external objects and provide valuable information after the initial phases of contact [1]. Compliance and softness also play a critical role in object grasping and manipulation [2].

Several behavioral studies investigated the mechanisms of touch-enabled compliance perception. Two mechanisms have been identified: cutaneous compliance perception, which is related to skin and fingerpad mechanical deformation, and kinesthetic sensing, which relates to the ability of the muscular-skeletal system to process forces and displacements [3], [4]. While both mechanisms are significant for softness perception, cutaneous cues are more prominent than kinesthetic ones, especially with deformable compliant objects [3], [4], [5]. Furthermore, in tasks such as grasping and manipulation, tactile cutaneous information provides fundamental feedback for control loops [6].

The complexity of human touch poses challenges when it comes to being mathematically modeled and replicated in engineering devices. Nevertheless, there is a significant interest in developing artificial systems with advanced tactile abilities, such as robotic hands for object exploration and manipulation.

The study of biological principles and biomimicry can guide the development of artificial systems with improved sensing capabilities by taking inspiration from the human touch. One promising example is the development of soft tactile optical sensors [7], [8], [9], which can help to estimate object properties relying on their functional similarities with the main working principles of human cutaneous sensing.

These sensors usually consist of a rubber membrane filled with gel and a camera that captures images of the deformed sensor surface upon contact with external objects, allowing inferring contact-related information. There are two main optical sensing techniques to retrieve the deformation depending on the sensor design: one measures the displacement of marked pins embedded in the sensor [10], and the other evaluates surface shading caused by internal light sources to retrieve the depth map via photometric stereo [11]. Combinations of these strategies also lead to approaches that rely on biological principles that characterize cutaneous sensing and touch perception in humans and mammalians [12].

These techniques have been successfully applied to enable object shape reconstruction, and object localization [13], [14], geometry and slip measurement [15], tactile object classification and grasp success

prediction [16], in-hand manipulation of unknown objects toward a stable grasp configuration [17].

However, soft tactile optical sensors have not been extensively used for compliance discrimination. In [13], the GelSight soft optical sensor was employed for estimating object compliance using deep learning techniques based on convolutional neural networks. Data-driven (DD) methods were chosen due to the challenges of creating a model of the sensor-object interaction due to the deformability of the sensor body. However, DD approaches have limitations in terms of the quality and dimensionality of the data used for training, as well as computational costs [18]. On the contrary, model-based methods could offer a more robust and cost-effective solution Furthermore, DD techniques usually discard the underpinning perception processes of human touch. When considering integrating optical tactile sensors with robotic hands and closing the action-perception loop in robotics-enabled prosthetics or telerobotics, this limitation becomes significant. Indeed, to achieve an effective sensory restoration through non-invasive wearable feedback, we need to provide the same kind of stimuli that natural touch perception commonly relies on, known as Modality Matching (MM) [19], using the same language of human tactile perception.

In this work, we introduce, for the first time, a model-based approach for compliance estimation by applying optical flow analysis to data retrieved via a soft biomimetic optical tactile sensor that mimics the human fingertip, TacTip [8], [12]. This estimation is based on computational models of human tactile perception, and more specifically on the observed contact area spread rate paradigm and tactile flow computation, which are derived from behavioral and neuroscientific studies on human haptics [12], [20]. Extensive scientific evidence indicates that humans use contact area growth to distinguish the compliance of objects [20]. The Contact Area Spread Rate (CASR) paradigm [20], states that human cutaneous sensing and perception of softness mainly rely on the spread of the contact area over the finger-pad under increasing indenting force. The increase of the contact area can be evaluated in terms of the flow of iso-strain energy density (SED) surfaces across the fingerpad volume, as formulated by the tactile flow model that represents the tactile counterpart of optical flow [21]. Increasing the indenting force causes a radial flow of the iso-SED surfaces from the center of contact, leading to an expansion of the contact area over the fingerpad. The dilation rate increases with softness and can be determined based on the divergence of the tactile flow. In this letter, we propose an indirect estimation of the tactile flow by computing the optical flow of images acquired by the TacTip sensor [8] during the indentation of silicone specimens with different levels of compliance. Then, the divergence of the optical flow, referred to the indenting force, is used to estimate the area variation during the contact. We show that with this biomimetic approach, we can discriminate compliance levels, both when the TacTip acts along the normal axis of the specimen surface and along an axis inclined w.r.t. the normal one. Providing an approximate relation between compliance and the CASR, we demonstrate that our strategy allows inferring the compliance of new unknown specimens.

II. The Biomimetic Approach

The main objective of this manuscript is to introduce a model-based approach rooted in human perceptual mechanisms, for object compliance discrimination with the TacTip, and validate it through benchtop experiments. The presented approach pries upon three main components: a soft biomimetic optical tactile sensor, computing optical flow from images captured by the sensor, and the connection between the divergence of the optical flow and the Contact Area Spread Rate (CASR) for discriminating softness.

A. Soft Biomimetic Optical Tactile Sensor

The TacTip (Fig. 1) is a tactile sensor inspired by the shallow layers of glabrous skin that reproduces the epidermis and the dermis with an outer layer of rubber and with an internal filling of elastomer gel respectively [8]. The gel layer also contains a system of rigid inner nodular pins endowed with markers that convert surface indentation into shear strain. This approach is unique because touch is detected only by shear strain through a marked pins' system. Analyzing the displacement and velocity of markers in the TacTip provides information similar to that provided by human mechanoreceptors in response to tactile stimuli. Markers' displacement gives information comparable to the ones provided by slow adaptive Merkel cells activated in stable contact conditions, as in shape, edge detection, and compliance [8], [22]. Meanwhile, the makers' velocity gives information similar to the ones processed by fast adaptive Meissner corpuscles in response to skin movement and changes in contact [23], [24], [25]. A more exhaustive description of the TacTip soft biomimetic optical tactile sensor can be found in [8], [12].

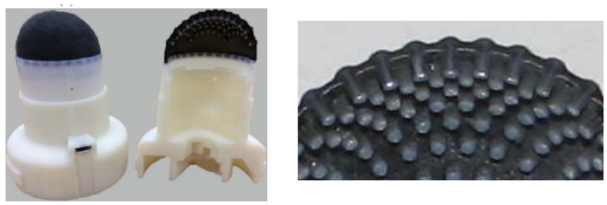

Fig. 1. Representation of TacTip internal structure [12].

B. Optical Flow Estimation

The pattern of an object's apparent motion in a visual scene arising from the relative motion between an observer and the scene is called *optical flow* [26], [27]. It can also be defined as the distribution of apparent velocities of brightness patterns in an image [28]. Optical flow plays a significant role in locomotion control and the perception of movement, distance, and shape of objects, as reported in several works [29], [30], [31]. In robotics, the optical flow has found numerous applications in fields such as navigation, image segmentation, motion detection, collision avoidance, time-to-contact estimation, and stereo-image disparity evaluation [32], [33], [34].

Optical flow relates the changes in pixels' brightness to the motion of the brightness patterns, assuming that the pixels' brightness of moving patterns is constant. Let $E(x, y, t)$ be the brightness of a pixel at location (x, y) at instant t the assumption of optical flow constancy can be stated as

$$E_x u + E_y v + E_t = 0 \tag{1}$$

where E_x, E_y, E_t are the partial derivatives of image brightness w.r.t. x, y, t, respectively, and $u(x, y, t) = \frac{\partial x}{\partial t}$, $v(x, y, t) = \frac{\partial y}{\partial t}$ are the optical flow components. Since the equation (1) has two unknowns, it can provide only the optical flow component along the brightness gradient. Then, the correct optical flow estimation is unachievable without additional information, as stated in the so-called *aperture problem*. This phenomenon is responsible for several perceptual illusions, among which we can find the well-known *Barber Pole Illusion* [35], which is the non-veridical perception of the motion direction of translating gratings. Computational approaches in the literature can be grouped into sparse and dense methods [36], [37], [38], [39]. Sparse methods require identifying trackable features such as corners and edges and are effective for tracking objects with specific characteristics. On the other hand, dense methods only require knowledge of pixel brightness and a constraint on the optical flow smoothness. Dense methods are useful when the flow of an entire region of a given brightness uniform pattern or the flow of the whole image is needed.

In our soft biomimetic optical tactile sensor, the displacement of one pin's marker is related to the movement of neighboring markers (see Section II-A). This allows transmission of the movement of the soft surface that produces a smooth outward or inward flow depending on the contact point. We adopted a dense optical flow estimation technique called the Horn-Schunck method to estimate the optical flow on the

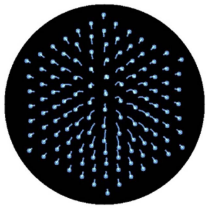

Fig. 2. Representation of optical flow due to the displacement of the pins in the TacTip sensor. Light blue circles represent the pin's position and the light blue lines show the trend of the optical flow.

entire TacTip sensible area (Fig. 2). This method adds a constraint on velocity to estimate the optical flow correctly; neighboring pixels have similar motion velocities, i.e., the velocity field of brightness patterns varies smoothly in the image. The estimation is obtained by finding the optical flow velocity pair (u, v) that minimizes a cost function expressed in terms of the sum of errors in evaluating the rate of change of image brightness and the measure of departure from smoothness in the velocity flow. The pair (u, v) is obtained by solving the two equations provided for each image pixel by (1) together with the constraint of smoothness, e.g., through the Gauss-Seidel iterative method, resulting in

$$\begin{aligned} u^{n+1} &= \bar{u}^n - E_x \left[E_x \bar{u}^n + E_y \bar{v}^n + E_t\right] / \left(\alpha^2 + E_x^2 + E_y^2\right) \\ v^{n+1} &= \bar{v}^n - E_y \left[E_x \bar{u}^n + E_y \bar{v}^n + E_t\right] / \left(\alpha^2 + E_x^2 + E_y^2\right). \end{aligned} \quad (2)$$

In (2) $\bar{u}$ and $\bar{v}$ are the difference between the pixel components and the weighted average of the neighboring pixels components, α prevents sudden adjustments of the estimated optical flow due the noise in the evaluation of the image brightness partial derivatives, and n is the number of iterations that should be larger than the number of pixels across the largest region of constant brightness. The image brightness partial derivatives E_x, E_y, E_t are estimated from the average of the first differences along four parallel edges of an eight measurements cube constructed w.r.t. the pixel and its neighborhood. Further details on Horn-Schunck method implementation can be found in [28].

C. Tactile Flow and Contact Area Spread Rate

In [21], [40], a computational model equivalent to optical flow in (1) called the *tactile flow model* was introduced to study the tactile perception of dynamic stimuli. This model extended the Horn-Schunck method to three-dimensional strain tensor distributions within the human fingerpad. The tactile flow model was shown to predict an illusory phenomenon in the tactile domain, analogous to the barber-pole effect in vision, during both passive [21] and active [41] exploration of textured surfaces. Tactile and optical flow have different interpretations of the involved quantities. In tactile flow, the image pixel coordinates (x, y) represent the spatial coordinates of a voxel element in the fingertip tissue, and the partial derivatives of image brightness E_x, E_y, E_t encode the tactile stimulus strength at a particular point (x, y) at time t. The perceived intensity of the tactile stimulus is quantified in terms of Strain Energy Density (SED), which is the scalar quantity that Merkel corpuscles, responsible for shape and compliance perception, are mainly sensitive to [21], [42].

In touch, regions on the fingertip that are subjected to an equivalent activation of Merkel corpuscles, hence, to the same strain energy density, are called Iso-SED contours. They can expand radially outward from the center of the contact area as the probing force increases. The radial patterns of stimuli on these contours can provide information on the compliance of probed objects, as demonstrated in the CASR paradigm. This expansion is similar to the radial patterns of iso-brightness contours used in vision to estimate the time-to-contact of an approaching object. The mathematical relation between the contact area dilatation and the tactile flow is

$$\frac{\mathrm{d}A_c}{\mathrm{d}F} = \oint_c \vec{\phi} \cdot \vec{\mathbf{n}} \, \mathrm{d}l = \iint_{A_c} \nabla \cdot \vec{\phi} \, \mathrm{d}A \quad (3)$$

where F is the force, A_c is the area comprised in the iso-SED contour c, $\vec{\phi} \cdot \vec{\mathbf{n}}$ is the SED flow vector component normal to the contour, and $\nabla \cdot \vec{\phi}$ is the *divergence* of the flow. Equation (3) shows that the stress-strain distribution in the fingertip is strongly influenced by the rheological properties of the touched object, which change significantly between soft and rigid items. This phenomenon is conceptualized in the so-called contact area spread rate (CASR) paradigm for softness perception [20], which can be regarded as the haptic counterpart of the rate of dilatation of the retinal image of an approaching object for the estimation of its time-to-contact with respect to the observer. The larger the rate of dilatation, the faster the object moves. The larger the CASR, the softer the object.

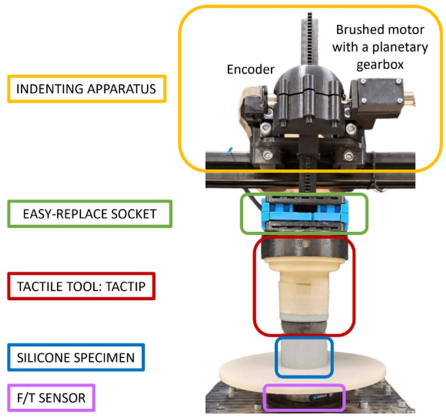

Fig. 3. Whole apparatus used both to characterize specimens' stiffness and in CASR validation experiment, composed of vertical moving support, the tactile tool, in the depicted case, the TacTip, fixed circular plate with an ATI force/torque sensor on the bottom.

D. Contact Area and Divergence

In time-to-contact experiments [43], the authors proposed a relation between the derivative of the area of a closed contour and the image divergence. Starting from

$$I_m = \iint_{a(t)} m(x, y) \, \mathrm{d}x\mathrm{d}y, \quad (4)$$

where I_m is the moment of area of a contour $a(t)$, and $m(x, y)$ is the scalar function of image position (x, y), and applying the flux transport theorem and Green's theorem, they obtained

$$\frac{\mathrm{d}I_m}{\mathrm{d}t} = \iint_{a(t)} \nabla \cdot (mn) \, \mathrm{d}x\mathrm{d}y \quad (5)$$

where n represents the normal component of image velocities. Choosing $m(x, y) = 1$ and assuming time independence and a linear field for the image velocities field, the derivative of the area can be evaluated as the product between the area $a(t)$ and the divergence $\mathscr{D}$:

$$\frac{\mathrm{d}a(t)}{\mathrm{d}t} = \iint_{a(t)} \nabla \cdot n \, \mathrm{d}x\mathrm{d}y = a(t)\mathscr{D}. \quad (6)$$

Since (6) is comparable to (1), this can be used to evaluate the CASR considering the derivative of the area with respect to the probing force. We built upon these results and the analogies between touch and vision to infer the compliance of silicone specimens probed with the TacTip sensor, exploiting the computation of the optical flow and its divergence to estimate the spread of contact area in the force domain.

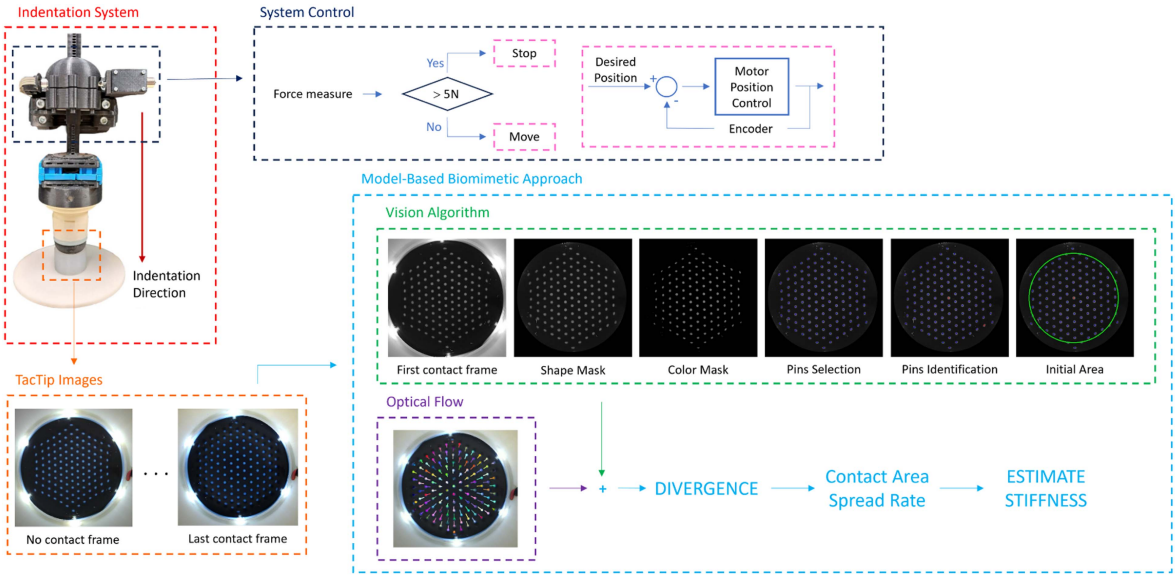

Fig. 4. Schematics describing the complete pipeline.

III. Methods

Once the dense optical flow $u(x, y)$ and $v(x, y)$ components have been obtained with the Horn-Schunk method from sequences of image frames retrieved with the TacTip camera, we compute their partial derivatives with respect to x and y through the 3-stencil technique:

$$\frac{\partial u}{\partial x} = \frac{1}{2}(u(x+1, y) - u(x-1, y))$$
$$\frac{\partial v}{\partial y} = \frac{1}{2}(v(x, y+1) - v(x, y-1)). \tag{7}$$

Exploiting the divergence theorem and its equivalence to Green's theorem in a two-dimensional case, the divergence $\mathscr{D}$ can be evaluated as the summation on the whole camera image of the sum of the optical flow partial derivatives

$$\mathscr{D} = \sum_{i=1}^{p_x \times p_y} \left(\frac{\partial u(x_i, y_i)}{\partial x} + \frac{\partial v(x_i, y_i)}{\partial y} \right) \tag{8}$$

where p_x and p_y are the pixel number along the x and y axis, respectively. Thus, we defined the cumulative divergence $\mathscr{D}_{\text{cum}}$ as the summation of the divergence of the dense optical flow in a frame sequence:

$$\mathscr{D}_{\text{cum}} = \sum_{j=1}^{f} \mathscr{D}_j \tag{9}$$

with f the number of frames in the analyzed sequence. Then, recalling the results of Cipolla and Blake [43], i.e., defining the integral of the optical flow divergence as equal to the cumulative divergence of the optical flow multiplied by the area,

$$\frac{\mathrm{d}A_c}{\mathrm{d}F} = \iint_{A_c} \mathscr{D}\, \mathrm{d}A = A_c \mathscr{D}_{\text{cum}}, \tag{10}$$

the contact area, correspondent to the probing force F_i at the i-th frame, can be evaluated as

$$A_{c_i} = A_{c_0} \exp(\mathscr{D}_{\text{cum}} F_i), \tag{11}$$

where $\mathscr{D}_{\text{cum}}$ is computed as in (9) with $f = i$ and A_{c_0} is the initial area estimated in the static condition of the TacTip. Since we are interested in the CASR, once we obtained the contact area value, we evaluated $\frac{\mathrm{d}A_{c_i}}{\mathrm{d}F_i}$ at frame i as,

$$\frac{\mathrm{d}A_{c_i}}{\mathrm{d}F_i} = \sum_{j=1}^{i} \frac{A_{c_j} - A_{c_{j-1}}}{F_j - F_{j-1}}, \tag{12}$$

taking into consideration $F_0 = 0$. Therefore, the CASR estimated on the whole frame sequence results as in (12) with $i = m$. We use the contact area spread rate, estimated for each frame sequence, to discriminate possible different levels of the softness of the explored objects. Indeed, fixing the probing force, higher CASR values correspond to higher levels of softness. This result suggests that the higher the CASR, the softer the object. Fig. 4 depicts a schematic of the complete method pipeline.

IV. Experiments

This section describes our experimental setup, inspired by [44], suitably designed to perform experiments and validate the proposed model-based approach. We also report the software implementation for data acquisition and method implementation. Finally, we describe the experiments we performed.

A. Experimental Setup

The objective is to indent a given specimen with an increasing probing force along the direction perpendicular to the top surface.

To this aim, we built the apparatus in Fig. 3 that consists of a system of cogwheels driven by a motor that controls the vertical movement of rigid support that ends with a square plate with an interlocking attachment to fast hook up the TacTip sensor or a rigid plate. The cogwheels system, support, and plate are made of ABS via rapid prototyping. We used a Maxon DCX8 DC brushed motor with a planetary gearbox GPX8 35:1 power supplied at 12 V and controlled by a qbrobotics board [45]. The controller is a position PD running at 1 kHz, whose gains, tuned following the Ziegler–Nichols method, are $K_{\text{p}} = 0.04$ and $K_{\text{d}} = 0.002$, respectively. An Auster Microsystem AS5045 encoder with a 12-bit resolution was used to compute the support position. The static part of the structure is positioned under the moving part and is composed of a circular 3D-printed smooth plate with a radius of 30 mm on which different specimens under exploration rest. Underneath this

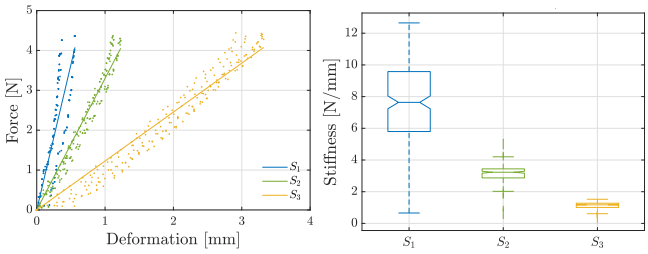

(a) Linear model of the stiffness fitting (b) Stiffness' Boxplot

Fig. 5. Stiffness discrimination based on linear force-deformation relation. Different specimens are color-coded, respectively, S_1 in blue, S_2 in green, and S_3 in yellow.

disc, an ATI Mini45 with a force resolution of 0.0625 N along the vertical axis z is fixed to measure the force.

B. Data Acquisition and Method Implementation

The data to be collected during the indentation of the TacTip on the specimen along the vertical axis are the force value measured by the ATI sensor, the support displacement computed thanks to the encoder information, and the images captured by the sensor's camera. The camera is a CMOS OV2710 Full HD 1080P web camera that can capture images at 100 fps with a 3.6 mm lens. Later we will refer to 'cycle' as a complete indentation on a single specimen at a fixed speed. A custom double-thread C++ software was realized for data acquisition. The main thread provides the motor's desired position based on the speed and collects the force data, the support actual position, and the camera image frame number, with a frequency of 200 Hz. The high-priority thread provides force filtering achieved with a moving average filter with a window of 5 elements, a cut-off frequency of around 5 Hz, and a delay of 0.5 s. The low-priority thread saves the TacTip grey-scale 300×300 pixel camera images with a sample rate of 20 Hz. Therefore a new camera image is obtained for every ten samples of the main thread. The images collected during one cycle are saved in a multi-page TIFF file.

A custom Python module that implements the method described in Section III was developed. The module includes three functions for evaluating dense optical flow and divergence, estimating the initial area, and computing area and CASR. The first function calculates the optical flow and divergence between consecutive frames retrieved from a multi-page TIFF file saved during one cycle, using Horn-Schunck parameters of $n = 26$, coherently with the maximum size in pixel of a TacTip pin, and $\alpha = 0.1$. The second function estimates the initial area required to solve (11), assuming that A_{c_0} is the area of the largest circle defined by the pins position of the TacTip in static conditions. This is achieved through a vision algorithm (Alg.1) that utilizes OpenCV libraries and takes into account the first frame of the image sequence, corresponding to no contact force, to estimate the interested area.

The third function implements the computation of area and CASR as described in Section III.

C. Performed Experiments

In the following experiments, we considered three cylindrical silicone specimens (S_1, S_2, S_3) (height: 40 mm, radius: 20 mm), realized by mixing a given quantity of Sylgard 184 silicone in different compositions. Therefore, the specimens present three different levels of stiffness $(S_1 > S_2 > S_3)$. Two experiments were conducted using different tactile tools to test the relationship between CASR and softness. The first experiment used an ABS smooth plate as a tactile tool to characterize the stiffness of the specimens, while the second experiment used the

Algorithm 1: Initial Area Estimation.

Step 1: Apply masks to initial frame for pins detection
$frame \leftarrow file.TIFF[0]$
$mask\_circle = cv.circle(mask)$
$mask\_color = cv.inRange(frame, low\_color, upp\_color)$
$frame \leftarrow frame + circle\_mask + color\_mask$
Step 2: Find pins contours and respective centroids
$edge = cv.Canny(frame)$
$contours, hierarchy = cv.findContours(frame)$
for i in range (0, len(contours)) **do**
  $c = contours[i]$
  $area = cv.contourArea(c)$
  $moments = cv.moments(c)$
  if moments["m00"] != 0 **then**
    $cX = int(moments[''m10''] / moments[''m00''])$
    $cY = int(moments[''m01''] / moments[''m00''])$
  else
    $cX, cY = 0, 0$
  $centroid.append(cX, cY)$
Step 3: Select the central pin and the furthest one
$central\_pin = [cX\_center, cY\_center]$
$distance = 0$
for i in range (len(centroid)) **do**
  $distance\_new = Euclidean(central\_pin, centroid[i])$
  if distance_new > distance **then**
    $radius = distance\_new$
  $distance = distance\_new$
Step 4: radius and area in mm with intrinsic camera matrix
$radius \leftarrow radius\_mm$
$a_0\_mm = pi * radius^2$

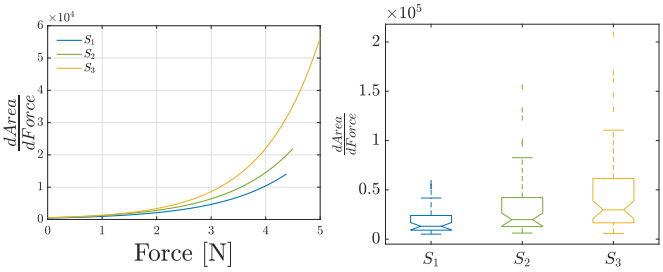

(a) Fitting of $\frac{dA_c}{dF}$ (b) Boxplot of $\frac{dA_c}{dF}$

Fig. 6. CASR discrimination based on the proposed model. Different specimens are color-coded, respectively, S_1 in blue, S_2 in green, and S_3 in yellow.

TacTip soft optical tactile sensor as a tactile tool to validate our novel model-based approach.

In the experiments, the speed of the tactile tool was kept constant at 5 mm/s to stay within the elastic domain of contacts where Hertz's theory applies. Indeed, if the loading rate is slow enough the stresses are in static equilibrium with the external loads at all times in the loading cycle, allowing neglect of the dynamic effects.

We tested the specimens five times to gather sufficient data for statistical analysis. The range of contact forces considered for each trial was from 0.5 N to 5 N, which is consistent with the normal loads associated with light touch perception in humans and mammalians [46]. The lower bound represents the moment when the tactile tool comes into contact with the specimen (*contact-on* condition), while the upper bound defines the end of the trial. During each test, the tactile tool moved towards the specimen along the vertical axis at a constant speed until the upper bound was reached. After, the tool came back to the start position and waited for 2 s before the new trial. For each trial, the raw and filtered contact forces, the desired and actual position of the support,

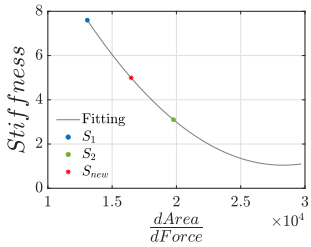

Fig. 7. $\kappa_{S_{new}}$ estimation considering fitted model on $\frac{\mathrm{d}A_c}{\mathrm{d}F}$ and κ Different specimens are color-coded, respectively, S_1 in blue, S_{new} in red, S_2 in green.

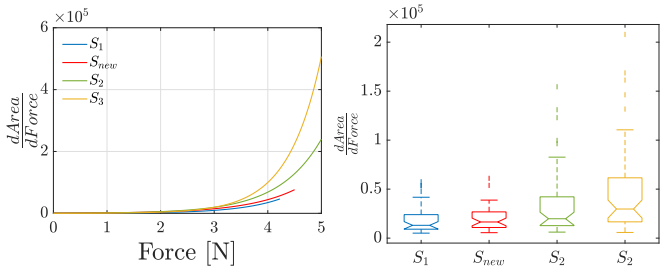

(a) Fitting of $\frac{\mathrm{d}A_c}{\mathrm{d}F}$ (b) Boxplot of $\frac{\mathrm{d}A_c}{\mathrm{d}F}$

Fig. 8. S_{new} CASR discrimination based on the proposed model. Different specimens are color-coded, respectively, S_1 in blue, S_{new} in red, S_2 in green, and S_3 in yellow.

and the associated camera frame index were saved for data analysis. The camera image sequence was saved only in the experiment with the TacTip. In addition to the experiment where the TacTip indented the specimen along its perpendicular axis, we tested our method by placing the specimens with their surfaces inclined at 30° and 45° degrees to the contact direction of exploration, with two different containers designed and 3D-printed for this purpose.

V. Results

The data collected in each trial were truncated in the range [0.5,5] N of the filtered contact force to take into account only what happens during the contact phase. Therefore, the contact forces were aligned to the *contact-on* threshold equal to 0.5 N, and the actual position to the observation correspondent to the contact-on condition in such a way as to interpret the position as a measurement of deformation.

The data collected during the experiment with the rigid plate as a tactile tool were used to estimate the stiffness κ for specimens' characterization relying on the relation between force F and deformation d, i.e., $\kappa = F/d$. For each specimen, the stiffness coefficient was estimated through a linear model fitted between filtered aligned contact force and deformation with the worst adjusted R-squared of 0.882. Fig. 5(a) reports the linear model of the stiffness fitting for each specimen, and Fig. 5(b) presents the boxplot of samples of stiffness values obtained for each specimen in all five trials. Both plots of the stiffness discrimination showed that the specimen stiffness decreased from S_1 to S_3, with estimated stiffness values of $\kappa_{S_1} = 7.6, \kappa_{S_2} = 3.1, \kappa_{S_3} = 1.1$ N/mm, respectively. From the One-sample Kolmogorov-Smirnov test, we found that our data do not have a Gaussian distribution; hence we applied a non-parametric Wilcoxon rank-sum test. Results show that specimens are statistically different with a p-value $= 9.91e-55$ in the worst case.

The data collected during the experiment performed with the TacTip as a tactile tool were the input of the functions implemented in the Python module that return the values of contact area and CASR for each trial and specimen. We considered all data collected for each specimen in the five trials to evaluate the independence between the samples.

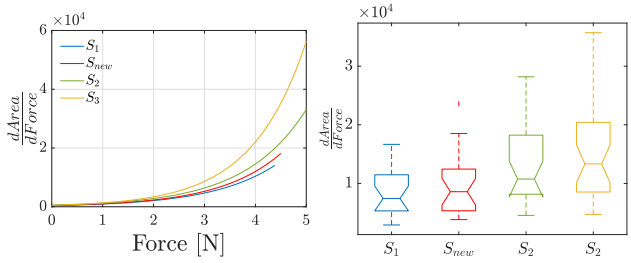

(a) Fitting of $\frac{\mathrm{d}A_c}{\mathrm{d}F}$ at 30° (b) Boxplot of $\frac{\mathrm{d}A_c}{\mathrm{d}F}$ at 30°

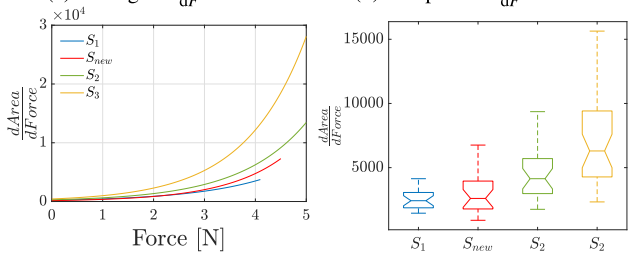

(c) Fitting of $\frac{\mathrm{d}A_c}{\mathrm{d}F}$ at 45° (d) Boxplot of $\frac{\mathrm{d}A_c}{\mathrm{d}F}$ at 45°

Fig. 9. S_{new} CASR discrimination based on the proposed model considering surface slope. Different specimens are color-coded, respectively, S_1 in blue, S_{new} in red, S_2 in green, and S_3 in yellow.

As is shown in Fig. 6(a), differences between CASR values were only evident when a sufficient force value was reached, which is consistent with human cutaneous object compliance recognition. For this reason, the data samples have been modified considering only the CASR values corresponding to force values greater than 2.5 N, and five more trials were performed for each specimen to ensure sufficient sample size. Based on the Kruskalwallis test, we can assert that the data samples are statistically different with a p-value $\approx 6.3e-5$, and the post-hoc lsd correction shows p-value ≈ 0.01 in the worst case. Fig. 6(b) presents the boxplot of each CASR evaluated on the data samples, showing that a good discrimination of the softness level can be obtained with the proposed model-based approach based on the contact area instead of on the deformation. The results demonstrate that lower stiffness values correspond to higher values of $\frac{\mathrm{d}A_c}{\mathrm{d}F}$.

Moreover, we created a new silicone specimen using the same procedure described in Section IV-C to demonstrate further our model's validity. Characterization with the rigid plate as a tactile tool resulted in a stiffness value of $\kappa_{S_{new}} = 5.3$ N/mm, which falls between the stiffness values of S_1 and S_2. We correctly provided these results with the proposed method. In particular, after evaluating the CASR values corresponding to the new specimen, we estimated $\kappa_{S_{new}}$ considering the relation between CASR and stiffness obtained by fitting previous CASR values and the respective stiffness for each specimen (Fig. 7). We found $\kappa_{S_{new}} = 4.99$ N/mm, thus making a mistake of 6% w.r.t. the value obtained with the deformation-force linear fitting.

Fig. 8 shows the correct discrimination of the new specimen reported in red both in the trend plot (Fig. 8(a)) and in boxplot (Fig. 8(b)), indeed the respective $\frac{\mathrm{d}A_c}{\mathrm{d}F}$ is between $\frac{\mathrm{d}A_c}{\mathrm{d}F}$ of S_1 and the one of S_2, as we expected.

Considering the results obtained with the experiments conducted by probing the specimen perpendicular to its surface, we tested our method by also placing the specimens with the surface inclined w.r.t. the contact direction of the TacTip.

Similar results were obtained by performing the same experiments and data analysis previously described. Looking at Fig. 9, the specimen S_1, S_2, S_3 are discriminated in the correct order also when the surface has a slope of 30° (Fig. 9(a), (b)) and of 45° (Fig. 9(c), (d)). In this case, the Kruskalwallis test rejects the null hypothesis, with p-value of the post-hoc lsd correction approximately equal to ≈ 0.01 and ≈ 0.005, respectively.

We tested the validity of our method in correcting estimating the stiffness of S_{new} also for these two object slopes, with the same procedure described before. For the 30° case, the estimated value of κ_{new} is equal to 3.95 N/mm and the error is about 25%; for the 45°, we obtained $\kappa_{new} = 6.8$ N/mm with an error of 28%, see Fig. 9. Both error percentages are expressed w.r.t. the value obtained with the force-deformation fitting.

VI. Discussions and Conclusions

This work introduces a novel model-based approach for discriminating compliance using soft tactile optical sensing. Our approach is based on the concepts of tactile flow and CASR and leverages the analogies between vision and touch. By computing the optical flow of images captured by a biomimetic soft optical sensor, i.e., the TacTip, and exploiting divergence as done in time-to-contact experiments, we were able to discriminate between different levels of object compliance. We also demonstrated the ability of our model to estimate the compliance of a new specimen both during normal indentation and along different directions. It is worth reporting that the results obtained with different object slopes are less favorable with respect to the normal indentation case. This outcome was anticipated considering that the optimal human movements, used to discern stiffness, also align perpendicularly to the object's surface [1]. We plan to address this point by combining our model-based approach with DD methods in future work through a careful design of the estimation methods that maximize the estimation outcomes while minimizing the computational costs. For what concerns the motivation of using tactile sensors with respect to kinesthetic ones, this moves from the observation that cutaneous information is the most informative when probing for softness deformable objects [5] and soft optical sensors offer unique advantages over other non-vision based techniques, in terms of resolution, flexibility, adaptability, and robustness [8], which make them ideal for the integration with soft robotic hands [47]. Furthermore, deformable compliant objects that exhibit the same force-deformation profile are indistinguishable relying on kinesthetic information only [3], but they can be easily discriminated in terms of compliance relying on the contact area spread rate. Thanks to our approach, we can retrieve contact area growth information, which can be also delivered for controlling skin stimulation using the same language of human tactile perception. This allows for an effective implementation of the Modality Matching approach for non-invasive sensory restoration in telerobotics and robotics-enabled prosthetics. To summarize, the focus of our manuscript is on proposing a model-based approach, well-grounded on computational models of human tactile perception, and validating it through benchtop experiments. Capitalizing on the successful experimental outcomes, we plan, as future work, the usage of the sensor with soft robotic grippers and with wearable haptics technology and extensive tests concerning autonomous robotic grasping of deformable objects as well as with robotics-enabled prostheses and telerobotics. These aspects, which are intriguing and represent the long-term goal of our research, are beyond the scope of our study - which is purely methodological and represents, as previously mentioned, the first biomimetic model-based approach for the retrieval of object compliance information with soft optical sensors, addressing the limitation of model-free methods related to the dependence on extensive and accurately labeled datasets, and paving the path to novel paradigms in the realm of haptic feedback.

References

[1] S. J. Lederman and R. L. Klatzky, "Relative availability of surface and object properties during early haptic processing," *J. Exp. Psychol.: Hum. Percep. Perform.*, vol. 23, no. 6, 1997, Art. no. 1680.

[2] T. Watanabe, "Softness effects on manipulability and grasp stability," in *Proc. IEEE/RSJ Int. Conf. Intell. Robots Syst.*, 2011, pp. 1398–1404.

[3] E. P. Scilingo, M. Bianchi, G. Grioli, and A. Bicchi, "Rendering softness: Integration of kinesthetic and cutaneous information in a haptic device," *IEEE Trans. Haptics*, vol. 3, no. 2, pp. 109–118, Apr./Jun. 2010.

[4] W. M. Bergmann Tiest and A. M. L. Kappers, "Cues for haptic perception of compliance," *IEEE Trans. Haptics*, vol. 2, no. 4, pp. 189–199, Oct.–Dec. 2009.

[5] M.A. Srinivasan and R. H. LaMotte, "Tactual discrimination of softness," *J. Neuriophysiol.*, vol. 73, no. 1, pp. 88–101, 1995.

[6] R. S. Johansson and G. Westling, "Signals in tactile afferents from the fingers eliciting adaptive motor responses during precision grip," *Exp. Brain Res.*, vol. 66, pp. 141–154, 1987.

[7] W. Yuan, S. Dong, and E. H. Adelson, "GelSight: High-resolution robot tactile sensors for estimating geometry and force," *Sensors*, vol. 17, no. 12, 2017, Art. no. 2762.

[8] B. Ward-Cherrier et al., "The TacTip family: Soft optical tactile sensors with 3D-printed biomimetic morphologies," *Soft Robot.*, vol. 5, no. 2, pp. 216–227, 2018, doi: 10.1089/soro.2017.0052, pMID: 29297773.

[9] K. Shimonomura, "Tactile image sensors employing camera: A review," *Sensors*, vol. 19, no. 18, 2019, Art. no. 3933.

[10] K. Kamiyama, K. Vlack, T. Mizota, H. Kajimoto, K. Kawakami, and S. Tachi, "Vision-based sensor for real-time measuring of surface traction fields," *IEEE Comput. Graph. Appl.*, vol. 25, no. 1, pp. 68–75, Jan./Feb. 2005.

[11] M. K. Johnson and E. H. Adelson, "Retrographic sensing for the measurement of surface texture and shape," in *Proc. IEEE Conf. Comput. Vis. Pattern Recognit.*, 2009, pp. 1070–1077.

[12] N. F. Lepora, "Soft biomimetic optical tactile sensing with the TacTip: A review," *IEEE Sensors J.*, vol. 21, no. 19, pp. 21131–21143, Oct. 2021.

[13] W. Yuan, C. Zhu, A. Owens, M.A. Srinivasan, and E. H. Adelson, "Shape-independent hardness estimation using deep learning and a GelSight tactile sensor," in *Proc. IEEE Int. Conf. Robot. Automat.*, 2017, pp. 951–958.

[14] M. Bauza, O. Canal, and A. Rodriguez, "Tactile mapping and localization from high-resolution tactile imprints," in *Proc. IEEE Int. Conf. Robot. Automat.*, 2019, pp. 3811–3817.

[15] S. Dong, W. Yuan, and E. H. Adelson, "Improved GelSight tactile sensor for measuring geometry and slip," in *Proc. IEEE/RSJ Int. Conf. Intell. Robots Syst.*, 2017, pp. 137–144.

[16] J. W. James, A. Church, L. Cramphorn, and N. F. Lepora, "Tactile model o: Fabrication and testing of a 3D-printed, three-fingered tactile robot hand," *Soft Robot.*, vol. 8, no. 5, pp. 594–610, 2021, doi: 10.1089/soro.2020.0019, pMID: 33337925.

[17] E. Psomopoulou, N. Pestell, F. Papadopoulos, J. Lloyd, Z. Doulgeri, and N. F. Lepora, "A robust controller for stable 3D pinching using tactile sensing," *IEEE Robot. Automat. Lett.*, vol. 6, no. 4, pp. 8150–8157, Oct. 2021.

[18] Y. Huang, M. Bianchi, M. Liarokapis, and Y. Sun, "Recent data sets on object manipulation: A survey," *Big data*, vol. 4, no. 4, pp. 197–216, 2016.

[19] K. Kim and J. E. Colgate, "Haptic feedback enhances grip force control of SEMG-controlled prosthetic hands in targeted reinnervation amputees," *IEEE Trans. Neural Syst. Rehabil. Eng.*, vol. 20, no. 6, pp. 798–805, Nov. 2012.

[20] A. Bicchi, E. P. Scilingo, and D. De Rossi, "Haptic discrimination of softness in teleoperation: The role of the contact area spread rate," *IEEE Trans. Robot. Automat.*, vol. 16, no. 5, pp. 496–504, Oct. 2000.

[21] A. Bicchi, E. P. Scilingo, E. Ricciardi, and P. Pietrini, "Tactile flow explains haptic counterparts of common visual illusions," *Brain Res. Bull.*, vol. 75, no. 6, pp. 737–741, 2008. [Online]. Available: https://www.sciencedirect.com/science/article/pii/S0361923008000117

[22] N. Cauna, "Nature and functions of the papillary ridges of the digital skin," *Anat. Rec.*, vol. 119, no. 4, pp. 449–468, 1954.

[23] N. F. Lepora, "Biomimetic active touch with fingertips and whiskers," *IEEE Trans. Haptics*, vol. 9, no. 2, pp. 170–183, Apr.–Jun. 2016.

[24] J. W. James, N. Pestell, and N. F. Lepora, "Slip detection with a biomimetic tactile sensor," *IEEE Robot. Automat. Lett.*, vol. 3, no. 4, pp. 3340–3346, Oct. 2018.

[25] N. Pestell and N. F. Lepora, "Artificial SA-I, RA-I and RA-II/vibrotactile afferents for tactile sensing of texture," *J. Roy. Soc. Interface*, vol. 19, no. 189, 2022, Art. no. 20210603.

[26] J. J. Gibson, *The Perception of the Visual World*. Berlin, Germany: Springer, 1950.

[27] N. Pestell and N. F. Lepora, "The theory of affordances," in *The Ecological Approach to Visual Percep.*. Boston, MA, USA: Houghton Mifflin Harcourt, 1977, ch. 8, pp. 127–137.

[28] B. K. Horn and B. G. Schunck, "Determining optical flow," *Artif. Intell.*, vol. 17, no. 1–3, pp. 185–203, 1981.

[29] K. Nakayama and J. M. Loomis, "Optical velocity patterns, velocity-sensitive neurons, and space perception: A hypothesis," *Perception*, vol. 3, no. 1, pp. 63–80, 1974.

[30] J. J. Gibson and L. Carmichael, *The Senses Considered as Perceptual Systems*, vol. 2, no. 1. Boston, MA, USA: Houghton Mifflin, 1966.
[31] H. C. Longuet-Higgins and K. Prazdny, "The interpretation of a moving retinal image," *Proc. Roy. Soc. London. Ser. B. Biol. Sci.*, vol. 208, no. 1173, pp. 385–397, 1980.
[32] S. S. Beauchemin and J. L. Barron, "The computation of optical flow," *ACM Comput. Surv.*, vol. 27, no. 3, pp. 433–466, 1995.
[33] A. Giachetti, M. Campani, and V. Torre, "The use of optical flow for road navigation," *IEEE Trans. Robot. Automat.*, vol. 14, no. 1, pp. 34–48, Feb. 1998.
[34] S. Baker, D. Scharstein, J. Lewis, S. Roth, M. J. Black, and R. Szeliski, "A database and evaluation methodology for optical flow," *Int. J. Comput. Vis.*, vol. 92, no. 1, pp. 1–31, 2011.
[35] N. Fisher and J. M. Zanker, "The directional tuning of the barber-pole illusion," *Perception*, vol. 30, no. 11, pp. 1321–1336, 2001.
[36] D. Fleet and Y. Weiss, "Optical flow estimation," in *Handbook of Mathematical Models in Computer Vision*. Berlin, Germany: Springer, 2006, pp. 237–257.
[37] A. Bruhn, J. Weickert, and C. Schnörr, "Lucas/Kanade meets Horn/Schunck: Combining local and global optic flow methods," *Int. J. Comput. Vis.*, vol. 61, no. 3, pp. 211–231, 2005.
[38] J.-Y. Bouguetet al., "Pyramidal implementation of the affine Lucas Kanade feature tracker description of the algorithm," *Intel Corporation*, vol. 5, no. 1–10, 2001, Art. no. 4.
[39] S. Baker, R. Gross, T. Ishikawa, and I. Matthews, "Lucas-Kanade 20 years on: A unifying framework: Part 2," *Int. J. Comput. Vis.*, 2003.
[40] E. Battaglia et al., "A finite element model of tactile flow for softness perception," in *Proc. IEEE 37th Annu. Int. Conf. Eng. Med. Biol. Soc.*, 2015, pp. 2430–2433.
[41] A. Moscatelli et al., "Touch as an auxiliary proprioceptive cue for movement control," *Sci. Adv.*, vol. 5, no. 6, 2019, Art. no. eaaw3121.
[42] K. O. Johnson, "The roles and functions of cutaneous mechanoreceptors," *Curr. Opin. Neurobiol.*, vol. 11, no. 4, pp. 455–461, 2001.
[43] R. Cipolla and A. Blake, "Surface orientation and time to contact from image divergence and deformation," in *Proc. 2nd Eur. Conf. Comput. Vis.*, 1992, pp. 187–202.
[44] D. Doria, S. Fani, A. Giannini, T. Simoncini, and M. Bianchi, "Enhancing the localization of uterine leiomyomas through cutaneous softness rendering for robot-assisted surgical palpation applications," *IEEE Trans. Haptics*, vol. 14, no. 3, pp. 503–512, Jul./Sep. 2021.
[45] C. Della Santina et al., "The quest for natural machine motion: An open platform to fast-prototyping articulated soft robots," *IEEE Robot. Automat. Mag.*, vol. 24, no. 1, pp. 48–56, Mar. 2017.
[46] S. Zhang et al., "Texture design for light touch perception," *BioSurface Biotribol.*, vol. 3, no. 1, pp. 25–34, 2017.
[47] B. Ward-Cherrier, J. Conradt, M. G. Catalano, M. Bianchi, and N. F. Lepora, "A miniaturised neuromorphic tactile sensor integrated with an anthropomorphic robot hand," in *Proc. IEEE/RSJ Int. Conf. Intell. Robots Syst.*, 2020, pp. 9883–9889.

Open Access funding provided by 'Università di Pisa' within the CRUI CARE Agreement